Phase transition to Bose-Einstein condensation for a Bosonic gas confined in a combined trap

Baolong Lü,[1] Xinzhou Tan,[1, 2] Bing Wang,[1, 2] Lijuan Cao,[1, 2] and Hongwei Xiong[1, *]

[1]*State Key Laboratory of Magnetic Resonance and Atomic and Molecular Physics,*
Wuhan Institute of Physics and Mathematics, Chinese Academy of Sciences, Wuhan 430071, People's Republic of China
[2]*Graduate School of the Chinese Academy of Sciences, Beijing 100049, People's Republic of China*

(Dated: November 22, 2010)

We present a study of phase transition to macroscopic superfluidity for an ultracold bosonic gas confined in a combined trap formed by a one-dimensional optical lattice and a harmonic potential, focusing on the critical temperature of this system and the interference patterns of the Bose gas released from the combined trap. Based on a semiclassical energy spectrum, we develop an analytic approximation for the critical temperature T_c, and compare the analytic results with that obtained by numerical computations. For finite temperatures below T_c, we calculate the interference patterns for both the normal gas and the superfluid gas. The total interference pattern shows a feature of "peak-on-a-peak." As a comparison, we also present the experimentally observed interference patterns of ^{87}Rb atoms released from a one-dimensional optical lattice system in accord with our theoretical model. Our observations are consistent with the theoretical results.

PACS numbers: 03.75.Lm, 67.25.dj, 37.10.Jk, 67.10.Ba

I. INTRODUCTION

Bosonic atoms confined in optical lattices have proved to be a unique laboratory for investigating quantum phase transitions from superfluids to Mott insulators [1–3]. The momentum distribution of a lattice system can be mapped out directly by the interference pattern of the atomic cloud after a ballistic expansion over a time of flight (TOF). The emergence of macroscopic bosonic superfluid is usually identified by the appearance of interference peaks. However, recent theoretical works [4, 5] for homogeneous gases in a three-dimensional (3D) lattice showed that this criterion of macroscopic superfluidity is not reliable since even a normal gas can have sharp interference peaks. The underlying physical picture is that a lattice system at finite temperatures possesses a "V-shaped" phase diagram [4–6] which includes a normal gas region between the Mott Insulator and the superfluid. The true signature of macroscopic superfluidity is the δ-function momentum peaks with nearly unit visibility [4]. Below critical temperature, the coexistence of superfluid and normal gas in the homogeneous lattice system should give rise to an interference pattern having a feature of "peak on a peak" [5]. The new criterion of macroscopic superfluidity makes it necessary to further investigate the phase transition of bosonic atoms in an optical lattice, particularly for the characteristics associated with the critical temperature and interference patterns. Experimental investigations are also required for comparison with relevant theoretical models.

There have been a few theoretical works [7–9] considering the translationally invariant (uniform) lattices. However, in a realistic experiment, an optical lattice is always accompanied by harmonic confinement in all dimensions, arising from the focused Gaussian laser beams and/or an external magnetic trap. A bosonic gas is, therefore, never spatially uniform over the lattice range. Wild *et al.* [10] have examined the critical temperature of the interacting bosons in a one-dimensional (1D) lattice with additional harmonic confinement. Ramakumar *et al.* [11] have investigated the condensate fraction and specific heat of non-interacting bosons in 1D, two-dimensional (2D), and 3D lattices in the presence of harmonic potentials. Based on a piecewise analytic density of states extended to excited bands, Blakie *et al.* [12] developed an analytical expression of the critical temperature for an ideal bosonic gas in the combined harmonic lattice potential, and compared the analytic result with their numerical computations. However, these studies on combined traps did not mention interference patterns of the released bosonic gases. A more recent theoretical paper [13] has investigated the Bose-Einstein condensation (BEC) in a 3D inhomogeneous optical lattice system, and predicted that a bimodal structure in the momentum-space density profile is a universal indicator of BEC transition.

The experiment of Spielman *et al.* [14] has examined the superfluid to normal transition for a finite-sized 2D optical lattice system. Their measurements confirm that bimodal momentum distributions are associated with the superfluid phase. For such a system with a typical density of 1 atom per lattice site, the phase transition behavior can be interpreted in terms of the commonly used Bose-Hubbard model.

Unlike the 2D and 3D cases, an inhomogeneous 1D optical lattice system is usually much more heavily populated, with an atomic number up to several hundreds in a single lattice site. In the superfluid phase, the on-site interaction energy U varies from site to site because of its dependence on the local population in single lattice sites. This increases the complexity in searching for

*Electronic address: xionghongwei@wipm.ac.cn

an analytical description of the phase transition. In this paper we present a study of the critical temperature and interference patterns of an ultracold bosonic gas confined by a 1D optical lattice and an additional magnetic potential. The interference patterns of the normal gas and the condensed atoms are treated separately. The superposition of the two parts gives rise to a feature of "peak on a peak." Different from a homogeneous lattice system, however, the normal gas can-not produce sharp interference peaks. Furthermore, the theoretical results are compared with our preliminary experiment for a 1D lattice system of ^{87}Rb Bose-Einstein condensates.

Our theoretical model relevant to the phase transition is for ideal bosonic gases. In fact, interatomic interaction may affect the shape of the interference pattern, especially for the condensed part which has a higher atomic density. In order to obtain a better match with the experiment result, we take the interaction energy into consideration for the condensed atoms during the time of flight. The computed result shows that interference peaks arising from the condensed atoms can be significantly broadened due to the interaction effect.

This paper is organized as follows. In Sec. II, we begin with a semiclassical energy spectrum for a combined harmonic lattice trap. Under the tight-binding approximation and in the low energy limit, we derive an analytical expression of the critical temperature for the atoms condensed to a superfluid state. The accuracy of the analytical results are checked with respect to the numerical calculations. Section III gives a description on how the interference patterns are calculated for the normal gas, as well as the Bose-condensed gas. In Sec. IV, we briefly introduce the experiment, and present the observed interference patterns for a comparison with our theoretical results. Finally in Sec. V, we summarize the obtained results.

II. CRITICAL TEMPERATURE

We now consider an ideal Bose gas confined in a 3D harmonic potential with axial symmetry around the z direction. The axial and transverse trapping frequencies are ω_z and $\omega_x = \omega_y = \omega_\perp$, respectively. Moreover, we assume that the axial confinement is much weaker than the radial confinement ($\omega_z \ll \omega_\perp$), so that the Bose gas is made cigar-shaped. A 1D optical lattice potential, $V_0 \sin^2(kz)$, is applied along the z axis, where $k = \pi/d$ is the wave vector of the lattice light, d denotes the lattice period, and V_0 denotes the potential depth of the lattice. V_0 can be written in terms of the recoil energy E_r, say, $V_0 = sE_r$, where $E_r = \hbar^2 k^2/2m$, and m is the atomic mass. The harmonic potential, together with the optical lattice, forms a combined trap written as

$$V(x,y,z) = \frac{1}{2}m\omega_\perp^2(x^2+y^2) + \frac{1}{2}m\omega_z^2 z^2 + V_0 \sin^2(kz). \quad (1)$$

In practice, an optical lattice is usually produced by a retro-reflected Gaussian laser beam which also produces a transverse confining potential, that can be simply absorbed into $\omega_\perp$ if it is non-negligible.

To obtain the eigenenergies of the combined trap system, one needs to derive the single-particle Hamiltonian of the system and then numerically diagonalize it [12]. Despite its accuracy for ideal Bose gases, this numerical method can not provide an analytic expression of the energy levels. The energy spectrum corresponding to the transverse confinement is described by equally spaced harmonic-oscillator states, whereas the oscillator treatment is not applicable to the axial dimension due to the presence of the optical lattice. Our discussion hereafter is based on the tight-binding approximation that only the ground band is accessible to the system. This approximation is valid when the thermal energy of the atoms is much less than the first band gap of a deep lattice. For a 1D uniform lattice, the eigen energy can be written as a function of quasimomentum q [15], $\epsilon(q) = \frac{1}{2}\hbar\widetilde{\omega} - 2J\cos(qd/\hbar)$. Here, $\widetilde{\omega}$ is the frequency of the local oscillation at each lattice well, while J is the tunneling energy due to the hopping to a nearest neighboring well, and it depends upon the lattice depth s in the following form [15]

$$J = \frac{4}{\sqrt{\pi}}E_r s^{3/4}\exp\left(-2\sqrt{s}\right). \quad (2)$$

It should be noted that Eq. (2) is valid only for deep lattices. At $s = 11$, for example, it overestimates J by approximately 18%. For the combined trap, it is a reasonable assumption that Eq. (2) remains valid as long as the trapping frequency ω_z of the weak axial confinement is much smaller than the tunneling rate $J/\hbar$. We are thus able to use a constant J over the entire lattice system at a given lattice depth. For simplicity the energy spectrum corresponding to the combined confinement in the axial direction is approximated by the semiclassical energy, $\epsilon(p_z) + \frac{1}{2}m\omega_z^2 z^2$, in the z-p_z phase space, where p_z is the quasimomentum in the ground band. Now we are able to write the total energy spectrum in an explicit form

$$\begin{aligned}\varepsilon_{n_x n_y}(z, p_z) = &\hbar\omega_\perp(n_x + n_y + 1) + \frac{1}{2}m\omega_z^2 z^2 \\ &+ \frac{1}{2}\hbar\widetilde{\omega}_z - 2J\cos(p_z d/\hbar),\end{aligned} \quad (3)$$

where $\{n_x, n_y\}$ are non-negative integers.

For a semiclassical description of this system, we treat the harmonic trap semiclassically while treating the optical lattice quantum mechanically. Such a picture corresponds to a density distribution of the thermal cloud:

$$n(z) = \sum_{n_x, n_y} \int \frac{dp_z}{2\pi\hbar} F(p_z, z) M d|\Phi_{p_z}(z)|^2, \quad (4)$$

where

$$F(p_z, z) = \frac{1}{\exp[\beta(\varepsilon_{n_x n_y} - \mu)] - 1},$$

and

$$\Phi_{p_z}(z) = \frac{1}{\sqrt{M}} \sum_{l=-M/2}^{M/2} w(z - ld) \exp\left(ip_z z/\hbar\right).$$

Here, Φ_{p_z} is the normalized wave function of a uniform optical lattice system with an extension of M lattice sites, and $w(z - ld)$ is the Wannier wave function. The total number of thermal atoms is then written as

$$\begin{aligned} N_{th} &= \int n(z)\mathrm{d}z \\ &= \sum_{n_x,n_y} \int \frac{\mathrm{d}p_z \mathrm{d}z}{2\pi\hbar} F(p_z, z) M d|\Phi_{p_z}(z)|^2. \end{aligned} \quad (5)$$

In the tight-binding limit, $w(z)$ is well localized within a single lattice site. In contrast, $F(p_z, z)$ is a slowly varying function of z. Therefore, $\Phi_{p_z}(z)$ in Eq. (5) can be integrated out. This results in a new integrand expressed as a summation of discrete $F(p_z, z - ld)d$, which in turn can be approximated as an integral over z. By doing so, one gets

$$N_{th} = \sum_{n_x,n_y} \int \frac{\mathrm{d}p_z \mathrm{d}z}{2\pi\hbar} F(p_z, z). \quad (6)$$

Below a critical temperature T_c the chemical potential μ of the Bose gas reaches the bottom of the ground band

$$\mu \to \mu_c = \hbar\omega_\perp + \frac{1}{2}\hbar\widetilde{\omega}_z - 2J,$$

while the lowest state with $p_z = 0$ becomes macroscopically populated which corresponds to the onset of Bose-Einstein condensation. The condensed atoms exhibit macroscopic superfluidity, whereas all other atoms beyond the lowest state form a so-called normal gas. Since the condensate is actually a quantum fluid, we use "superfluid" just as a synonym of BEC. The atomic number of the normal gas is given by the sum,

$$N_{nc} = N - N_c = \sum_{n_x,n_y} \int \frac{1}{\exp[\beta(\varepsilon_{n_x n_y} - \mu_c)] - 1} \frac{\mathrm{d}p_z \mathrm{d}z}{2\pi\hbar}, \quad (7)$$

where N is the total number of the atoms, N_c the atomic number of the condensed part, $\beta = 1/k_B T$, and k_B the Boltzmann constant. The integrand can be expanded in powers of the exponential term using the formula $1/(e^x - 1) = \sum_{n=1}^{\infty} e^{-nx}$. Moreover, the sum over n_x, n_y can be replaced by an integral if the atomic number N is large. Performing the integration over n_x, n_y as well as that over the coordinate z, one gets

$$\begin{aligned} N - N_c =& \frac{1}{(\beta\hbar\omega_\perp)^2} \sum_{n=1}^{\infty} \frac{1}{n^2} \left(\frac{2\pi}{n\beta m\omega_z^2}\right)^{1/2} \\ &\times \int \frac{\mathrm{d}p_z}{2\pi\hbar} \exp[-n\beta(2J - 2J\cos(p_z d/\hbar))], \end{aligned} \quad (8)$$

and the right side is a function of temperature T. Apparently, Eq. (8) is suitable for numerical calculation of the atomic number in the normal gas since the integration can be simply replaced by a summation over the p_z region.

By imposing that $N_c = 0$ at the transition, Eq. (8) determines a critical temperature T_c for a given N. Apparently, to obtain the value of T_c, one needs to carry out numerical computations based on Eq. (8). Nevertheless, we can derive an analytic expression of T_c in a limiting case. When the temperature of the Bose gas is so low that most atoms occupy the states in the vicinity of the bottom of the ground band, the relation $p_z \ll \hbar/d$ holds, and the cosine function in Eq. (8) can be expanded to the order of p_z^2. With the p_z-dependent function integrated out, one has

$$N = (k_B T_c/\hbar\overline{\omega})^3 (m^*/m)^{1/2} \zeta(3),$$

where $\overline{\omega} = (\omega_\perp^2 \omega_z)^{1/3}$ is the geometric average of the trapping frequencies, $m^* = \hbar^2/2Jd^2$ the effective mass of the atom, and $\zeta(\alpha) = \sum_{n=1}^{\infty} 1/n^\alpha$ the Riemann zeta function. Finally, one gets

$$k_B T_c = 0.94\hbar\overline{\omega}N^{1/3} (m/m^*)^{1/6}, \quad (9)$$

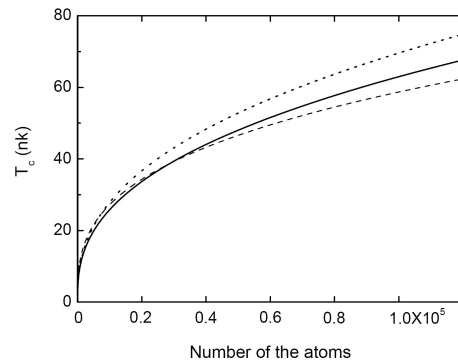which can be used as an analytic estimation of the critical temperature.

FIG. 1: Critical temperature T_c versus the total number of ^{87}Rb atoms. The solid curve and the dashed curve are obtained from the numerical calculation of Eq. (8) and the analytical approximation of T_c (Eq. (9)), respectively. The dotted line gives the full numerical result by diagonalizing the single-particle Hamiltonian. The lattice parameters are $d = 400\,\text{nm}$ and $s = 11.2\,E_r$. The trapping frequencies of the harmonic potential are $\omega_\perp = 2\pi \times 83.7\,\text{Hz}$ and $\omega_z = 2\pi \times 7.63\,\text{Hz}$, respectively.

We recall that an ideal Bose gas trapped in a 3D harmonic potential undergoes the phase transition to Bose-Einstein condensation at a temperature [16] $k_B T_c = 0.94\hbar\overline{\omega}N^{1/3}$. Comparing this expression with Eq. (9), one can see that T_c is changed by a factor of $(m/m^*)^{1/6}$ due to the presence of the 1D lattice. Since m^* is always larger than m [4] under tight-binding approximation, the

combined trap T_c is actually reduced compared to the case without lattice. Note also that a homogeneous 3D lattice system has a reduced T_c as well [4], but with a reducing factor $\sqrt{m/m^*}$ instead.

We have calculated the critical temperature T_c for a ^{87}Rb gas in the combined trap (see Fig. 1). The trap parameters are intentionally chosen to match our experiment which will be described in the later section. The numerically calculated T_c is displayed by the solid curve, while the dashed curve is the analytic T_c calculated according to Eq.(9). The discrepancy between the two curves becomes larger as the atom number N is increased, showing that the accuracy of the analytic estimation becomes worse for larger N. We thus use only the numerically calculated T_c in the following computations.
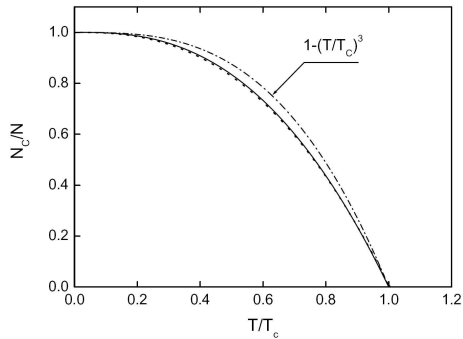

FIG. 2: Condensate fraction as a function of T/T_c. Solid line, numerical results based on Eq. (8). Dotted line is the full numerical result based on diagonalizing the single-particle Hamiltonian. The dash dot line is $1 - (T/T_c)^3$ for $T \leq T_c$. The parameters of the combined trap are the same as in Fig. 1, and the atomic number is $N = 5 \times 10^4$, corresponding to $T_c = 47.9$ nK.

It is well known that an ideal Bose gas in a 3D harmonic potential shows a T dependence of the condensate fraction as $N_c \sim 1 - (T/T_c)^3$ for $T < T_c$. We have also calculated the condensate fraction for our combined trap system with 5×10^4 atoms, as shown by the solid line in Fig. 2. It displays a noticeable deviation from the curve of $1 - (T/T_c)^3$, but fits well to the characteristic shape, $1 - (T/T_c)^\alpha$, with $\alpha = 2.679$.

To justify our analytical approximation, we also calculate the critical temperature and condensate fraction based on the diagonalization of the single-particle Hamiltonian. The energy spectrum of the system is written as

$$\varepsilon_{n_x n_y n_z} = \hbar\omega_\perp (n_x + n_y + 1) + \varepsilon_{n_z}. \qquad (10)$$

ε_{n_z} can be obtained numerically from the following single-particle Hamiltonian along the z direction,

$$\widehat{H}_z = -\frac{J}{2} \sum_{\langle i,j \rangle} \left(\widehat{a}_i^\dagger \widehat{a}_j + \widehat{a}_i \widehat{a}_j^\dagger \right) + \sum_i \varepsilon_i \widehat{a}_i^\dagger \widehat{a}_i. \qquad (11)$$

Here ε_i describes an energy offset at each lattice site due to the presence of the harmonic trap along the z direc-

tion. By diagonalizing the matrix $\left\langle i \left| \widehat{H}_z \right| j \right\rangle$, one can get directly the energy spectrum ε_{n_z}. Furthermore, with the following formula,

$$N = \sum_{n_x, n_y, n_z} \frac{1}{e^{\left(\varepsilon_{n_x n_y n_z} - \mu\right)/k_B T} - 1}, \qquad (12)$$

we give the full numerical results of the critical temperature and condensate fraction by the dotted lines in Figs. 1 and 2, respectively. Clearly, our semiclassical treatment agrees with the full numerical method, and proves to be reliable. Furthermore, it offers a convenient way to analyze the spatial distribution of a confined atomic cloud, which in turn simplifies the calculation of interference patterns.

III. INTERFERENCE PEAKS

When the combined trap is suddenly shut off at the moment $t = 0$, the Bose gas starts to expand freely. After a time of flight τ, the expanded wavepackets initially localized in single lattice wells overlap with each other, forming a 3D density distribution. In the following calculation, the x and y dependence of the atomic density will be integrated out so as to obtain a density profile along the z direction only. This is convenient for making a comparison with the experimental results. Usually, an absorption image is used to record the column density profile of a released atomic cloud. Supposing that the probe laser beam is applied along the direction of the x axis, the density profile along z can be easily obtained by integrating the column density over the y dimension.

A. Normal gas

In the combined trap, normal gas atoms are distributed over the transverse harmonic modes labeled by a positive quantum number $q = n_x + n_y$. For a given q, there are $q + 1$ degenerate states, and we hereafter call them substates. The summation over n_x and n_y in the previously mentioned equations is thus equivalent to $\sum_q (q+1) \cdots$. From Eq. (7), one sees that the substates belonging to the same q number have identical populations and spatial distribution along the z direction. Due to optical lattice potential, atoms in a single substate are further distributed over the Bloch states with different quasimomentum p_z with $p_z/\hbar \in (-\pi/d, \pi/d)$. Each p_z component can be treated semiclassically where the influence of the optical lattice is given by a quantum wave packet description, while the influence of the harmonic trap along the z direction is treated semiclassically. In such a picture, the single-particle wave function of a p_z component at $t = 0$ takes the following form:

$$\Psi_{p_z}^q(t=0) = \sum_l \alpha_l^q w(z - ld) \exp(ip_z z/\hbar), \qquad (13)$$

where $(\alpha_l^q)^2$ denotes the probability for a particle roughly located in the lth lattice site for the transverse harmonic mode q.

Equation (7) shows that the atomic density of a substate with p_z has an envelope as

$$n(z) = \frac{\Delta p_z}{2\pi\hbar} \frac{1}{e^{\beta[q\hbar\omega_\perp + 2J(1-\cos(p_z d/\hbar)) + \frac{1}{2}m\omega_z^2 z^2]} - 1}, \quad (14)$$

where Δp_z denotes a small interval of p_z. The atom number in the lth lattice site is then

$$n_l = \frac{d\Delta p_z}{2\pi\hbar} \frac{1}{e^{\beta[q\hbar\omega_\perp + 2J(1-\cos(p_z d/\hbar)) + \frac{1}{2}m\omega_z^2 d^2 l^2]} - 1}. \quad (15)$$

Therefore, α_l^q is simply given by $(\alpha_l^q)^2 = n_l/N_q$, with $N_q = \sum_l n_l$ being the total atom number of the p_z component in the substate of interest. In principle, α_l^q should be determined by solving the Schrodinger equation of H_z. However, as shown lately, the thermal average of in-trap density written in terms of $|\alpha_l^p|^2$ is matched to the expression obtained by semiclassical approximation, hence within semiclassical approximation $|\alpha_l^q|^2$ can be identified to $(\alpha_l^q)^2 = n_l/N_q$.

In the tight-binding limit $w(z)$ can be well approximated by a Gaussian wave packet $(\pi\sigma^2)^{-1/4}\exp(-z^2/2\sigma^2)$, where $\sigma = \sqrt{\hbar/m\widetilde{\omega}_z}$ is the oscillator length. After the free expansion over a time of τ, the single-particle wave function of the atoms with p_z is written as

$$\begin{aligned}
&\Psi_{p_z}^q(t = \tau) \\
&= \sum_l \alpha_l^q \int K(z, z', \tau) w(z' - ld) \exp(ip_z z'/\hbar) \mathrm{d}z'. \quad (16)
\end{aligned}$$

Here, $K(z, z', \tau) = \langle z| \exp(-iH\tau/\hbar)|z'\rangle$ is the propagator, with H the Hamiltonian governing the expansion process. If the interatomic interaction is neglected, H contains only the kinetic energy, say, $H = P_z^2/2m$. In this case, it is straightforward to get

$$K(z, z', \tau) = \sqrt{\frac{m}{i2\pi\hbar\tau}} \exp\left[\frac{im}{2\hbar\tau}(z - z')^2\right]. \quad (17)$$

For simplicity of expression and calculation, we will use dimensionless units for the length in z, the quasimomentum p_z and the time t by the replacement $z \to zd$ (and hence $\sigma \to \sigma d$), $p_z \to p_z\hbar/d$, and $t \to t(2md^2/\hbar)$. Inserting Eq. (17) into Eq. (16), and working out the integration over z', one gets

$$\Psi_{p_z}^q(t = \tau) = A\sum_l \alpha_l^q B(p_z, l, z), \quad (18)$$

with A and B given by

$$A = \pi^{-1/4}(\sigma + i2\tau/\sigma)^{-1/2},$$

$$B(p_z, l, z) = \exp\left[\frac{-2\tau\sigma^2 p_z^2 + 2\sigma^2 zp_z + i[4lp_z\tau + (z-l)^2]}{2(\sigma^4 + 4\tau^2)/(2\tau + i\sigma^2)}\right].$$
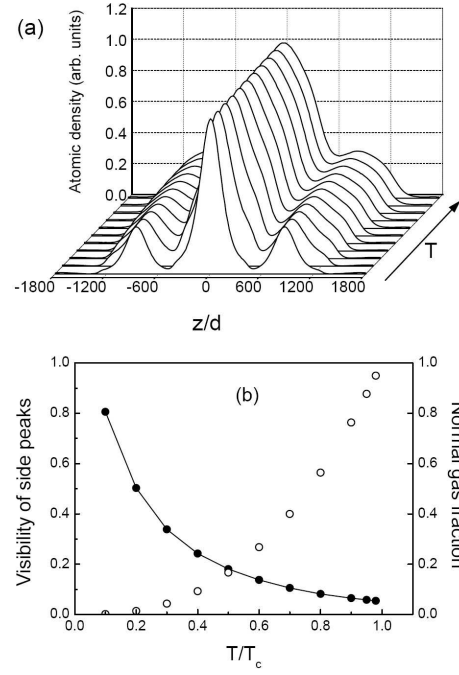

FIG. 3: (a) The solid lines are the calculated atomic distribution of the normal gas (^{87}Rb) after 30 ms of time of flight. The total atom number $N = 5.9 \times 10^4$, and the trap parameters are the same as in Fig. 1, corresponding to $T_c = 51.1$ nK. For the top two curves, the temperature T/T_c is 0.98 and 0.95, respectively. The other nine curves, from top to bottom, are for T/T_c ranging from 0.9 to 0.1 with a step of 0.1. Vertical scales of the curves have been adjusted so that the central peaks have roughly the same height. (b) Solid circles represent the visibility of the side peaks in (a). The solid curve connecting the points is added to guide the eye. Open circles show the normal gas fraction for the given total atom number.

Taking into consideration all transverse modes and all p_z components, one gets the atom density after the time of flight,

$$\begin{aligned}
n_{nc}(z) &= \sum_{q=1}^\infty \sum_{p_z} (q+1)N_q|\Psi_{p_z}^q(t=\tau)|^2 \\
&= |A|^2 \sum_{q=1}^\infty \sum_{p_z} (q+1)\left|\sum_l \sqrt{n_l} B(p_z, l, z)\right|^2. \quad (19)
\end{aligned}$$

In the numerical calculations of Eq. (19), the summation over transverse modes is cutoff at $q = 200$, while n is cutoff at 30 and lattice number l at ± 350. These cutoff numbers are chosen to assure a high accuracy better than 0.2% in the calculations of atom numbers. By setting Δp_z to 0.05π, the whole p_z range is divided into 40 intervals. This step size of p_z has the order of h/dM, where $M \simeq 100$ is the typical spatial extent in the z direction. We have also checked that the calculated results have almost no change when further reducing Δp_z. The step size in z is set to be $18d$ (7.2 μm), comparable to the

pixel size of $9\,\mu$m in our experiment.

In Fig. 3(a) we show the numerical results of a normal gas of ^{87}Rb atoms after $30\,$ms of time of flight. It is obvious that the normal gas leads to three peaks in the atomic distribution along the z dimension. However, these peaks are not sharp, and, close to the T_c, the side peaks are not even well resolved. In contrast, a normal gas initially trapped in a 3D homogenous lattice system gives rise to much sharper peaks [4].

We now define a visibility for the side peaks as in Ref. [17]:

$$v = \frac{n_A - n_B}{n_A - n_B}, \qquad (20)$$

where n_A is the atomic density of the side peak, and n_B is atomic density at the minimum between the central peak and the side peak. From Fig. 3(b) it can be seen that the visibility v is well below 1 at a considerable fraction of the normal gas. Although v can reach 0.8 at a very low temperature of $T = 0.1T_c \sim 5\,$nK, only about 0.1% of the atoms remain in the normal gas state while all other atoms are condensed. Actually, it is hard to detect such a small number of atoms using the conventional absorption imaging method.

B. Condensed gas

Unlike the normal gas, Bose-condensed atoms in the combined trap occupy the lowest state of $q = 0$ and pile to a small quasimomentum interval of $p_z = 0$. Nevertheless, the normal gas propagator holds also for the condensed gas. In analogy with the calculations for the normal gas, one can derive the single-particle wave function of the condensed gas after the time of flight,

$$\Psi_0(t = \tau) = A(\tau) \sum_k \alpha_k B_0(k, z), \qquad (21)$$

where k denotes the kth lattice well, α_k^2 is the probability of an atom staying in the kth well, and

$$B_0(k, z) = \exp\left[\frac{(i2\tau - \sigma^2)(z - k)^2}{2(\sigma^4 + 4\tau^2)}\right].$$

Note that, in the two formulas above, τ, z and σ are in their dimensionless form.

In the tight-binding limit, condensed atoms in the combined trap form an array of subcondensates along the z axis. Each subcondensate is a 2D quantum gas in nature, and its density distribution in the radial dimensions is described by a Thomas-Fermi profile [18]. The local chemical potential associated with the repulsive interaction of the atoms depends upon the average atom number in the following form [19]:

$$\mu_k^{\mathrm{loc}} = \sqrt{\frac{gm\omega_\perp^2 N_k}{\sqrt{2}\pi^{3/2}\sigma}}. \qquad (22)$$

Here, N_k is the average atom number in the kth lattice well, and $g = 4\pi\hbar^2 a/m$ is the interaction parameter with a the s-wave scattering length. The sum of μ_k^{loc} and the external harmonic potential $(1/2)m\omega_z^2 z^2$ is just the chemical potential which should remain invariant throughout the entire condensed gas at equilibrium. Accordingly, N_k is given by

$$N_k = (15N_c/16k_M)(1 - k^2/k_M^2)^2, \qquad (23)$$

where k_M labels the outermost lattice well populated with condensed atoms, and it is written as [18]

$$k_M^2 = \frac{2\hbar\overline{\omega}}{m\omega_z^2 d^2}\left(\frac{15N_c}{8\sqrt{\pi}}\frac{a}{a_{ho}}\frac{d}{\sigma}\right)^{2/5}. \qquad (24)$$

If we neglect the mean-field interaction of the condensed gas during the free expansion time, the density distribution after the TOF can be directly derived from the coherent superposition of the expanded subcondensates:

$$n_c(z) = |A(\tau)|^2\left|\sum_{k=-k_M}^{k_M}\sqrt{N_k}B_0(k, z)\right|^2. \qquad (25)$$

For the condensed gas before expansion, due to the high atomic density, μ_k^{loc}/h is in the order of several hundred Hertz. Although the atomic density drops quickly during the TOF, we still expect that mean-field interaction might lead to a considerable change in the coherence property of the expanding atomic clouds. For simplicity, we only consider the mean-field interaction within the single expanding subcondensates, and neglect the interaction between them. At the beginning of the TOF, the combined trap is suddenly turned off. Therefore, the total energy of the kth subcondensate includes only the mean-field energy at this moment, that is,

$$E_k = E_{\mathrm{int}} = (1/2)U_k N_k^2.$$

Here, $U_k = g\int|\Phi_k(\mathbf{r}, z)|^4 \mathrm{d}z\mathrm{d}\mathbf{r}$ is the on-site interaction matrix element of the kth subcondensate when confined in the combined trap. Using the analytic form of $\Phi_k(\mathbf{r}, z)$, we can get the expression of U_k in terms of the trap parameters:

$$U_k = \frac{1}{3}\left(\frac{2}{\pi}\right)^{3/4}\sqrt{\frac{gm\omega_\perp^2}{\sigma N_k}}. \qquad (26)$$

Its dependence on N_k is due to the fact that the atomic number affects the Thomas-Fermi radius of the radial wave-function. At later times, the total energy E_k remains constant despite the fact that the interaction energy is being converted into kinetic energy. Then, the corresponding chemical potential is simply given by $\mu_k = \partial E_k/\partial N_k = \mu_k^{\mathrm{loc}}/2$. Over the total time of flight, the kth subcondensate acquires an additional phase factor $\exp(-i\mu_k\tau/\hbar)$. Consequently, we can write the density distribution at the end of TOF by just inserting this

phase factor into Eq.(25):

$$n_c(z) = |A(\tau)|^2 \left| \sum_{k=-k_M}^{k_M} \sqrt{N_k} \exp(-i\mu_k\tau/\hbar)B_0(k,z) \right|^2.$$
(27)

From this equation one sees that μ_k will affect $n_c(z)$ by its nonuniformity. In Fig. 4(a), we plot two curves calculated, respectively, with Eqs. (25) and (27) for a condensed gas of 2.5×10^4 atoms. When the mean-field interaction is included, all three interference peaks are significantly broadened by about a factor of two. Since the mean-field interaction is nonnegligible, all the theoretical interference patterns mentioned hereafter are computed by Eq. (27).
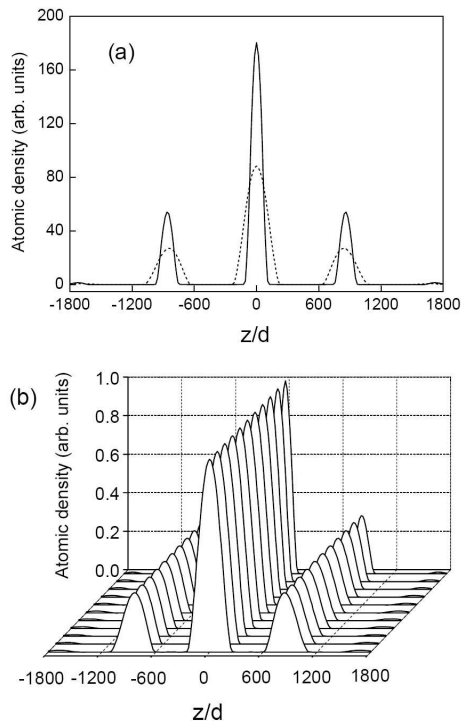

FIG. 4: Atomic distribution of the condensed gases after 30 ms of time of flight. The total atom number and the trap parameters are the same as in Fig. 3. (a) The dashed (solid) line is the result for $T = 0.7T_c$ with (without) a consideration of the mean-field interaction during TOF. (b) These curves are calculated from Eq. (27). From the top curve to the bottom one, the temperature is decreased in sequence, with the same values as in Fig. 3. Vertical scales of the curves have been adjusted so that the central peaks have the same height.

In Fig. 4(b), we plot the calculated density distributions of the condensed gases at different temperatures for a fixed total atomic number and a fixed lattice depth. With decreased temperature, the condensate contains more atoms, leading to wider interference peaks due to mean-field interactions. Unlike a normal gas, a condensed gas always shows fully resolved interference peaks, with a high visibility very close to 100%. This characteristic behavior can be easily understood as the global

coherence of condensed atoms in a superfluid state. Additionally, these peaks are considerably narrower than that of the corresponding normal gases, except the extreme cases of very low temperatures that the normal-gas atom number is very small and hardly detectable. When one measures the interference pattern of a mixture of the condensed gas and a normal gas, one would see three narrow peaks riding on three broad peaks. This is the so-called "peak on a peak" structure which was first predicted for a homogeneous system [4, 5]. For an inhomogeneous system in the combined tap, the onset of the condensed gas is also characterized by the "peak on a peak" structure.

On the other hand, if the condensed gas undergoes only a ballistic expansion during the TOF (no mean-field interaction), the relative intensity of the side peaks with respect to the central one should obey a simple law [18]: $P_1 = \exp(-4/\sqrt{s})$. We check the data in Fig. 4(b) ($P_1 = 0.303$ for $s = 11.2$), and find that the side peak intensities agree well with P_1 (to within 2 percent). It seems that the analytic expression of P_1 is also valid in the case of the existence of mean-field interaction during the expansion time.

IV. EXPERIMENT

In experiment, we create a cigar-shaped ^{87}Rb condensate in the hyperfine state $|F = 2, M_F = 2\rangle$, confined in a conventional Quadrupole Ioffe Configuration (QUIC) trap with an axial trapping frequency of $\omega_z = 2\pi \times 18.7$ Hz and radial trapping frequency of $\omega_\perp = 2\pi \times 205$ Hz. A nearly pure condensate contains approximately 2×10^5 atoms. If the frequency of the rf knife for evaporation cooling is ramped down further, we can obtain a condensate with a lower temperature at the cost of decreased atomic numbers. Certainly, the temperature is hard to measure because there are almost no thermal atoms remained. Nevertheless, we are able to coarsely adjust the temperature of the cold atomic sample using the rf knife. After the evaporation cooling, the QUIC trap is adiabatically relaxed until the axial and radial trapping frequencies are lowered to $\omega_\perp = 2\pi \times 83.7$ Hz and $\omega_z = 2\pi \times 7.63$ Hz, respectively. Accordingly, the spatial extension of the condensate wave packet is increased by a factor of 2.45, so as to cover more lattice periods at later times. The optical lattice is formed by one retroreflected laser beam which is derived from a Ti:sapphire laser at a wavelength of $\lambda = 800$ nm and focused to a $1/e^2$ radius of $300\,\mu$m. It is applied to the condensate along the long axis, and it is ramped up to a given intensity over a time of 50 ms and held at this value for 10 ms. The sum of the optical lattice and the QUIC trap potential gives a combined trap in accord with Eq. (1). The potential depth of the optical lattice is calibrated using the method of Kapitza-Dirac scattering [17]. We then suddenly switch off the combined trap and allow the cold atomic sample to expand freely for a time of 30 ms. Finally, we take an absorption image of the expanded atomic gas using a

CCD camera, from which we can deduce both the total atom number and the atomic density distribution.
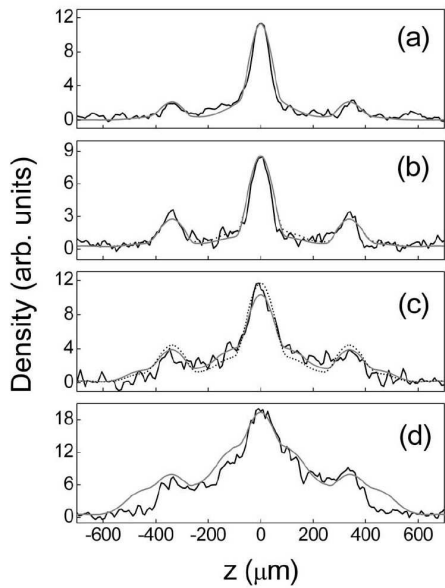

FIG. 5: Density distribution of two typical atomic samples of ^{87}Rb. Black curves are the measured linear density of the released ^{87}Rb atoms after a $30\,ms$ TOF. Gray curves are the calculated results based on Eqs. (19) and (27), where temperature is used as a fitting parameter. The dotted curves in (b) and (c) are the calculated results based on measured temperature values. Their vertical scales have been adjusted for comparison with the black curves. (a) The measured total atom number and lattice depth are $N \simeq 5.3 \times 10^4$ and $s \simeq 5.6$, respectively, corresponding to $T_c = 55.9\,$nK. $T = 44.7\,$nK is assumed in the computation. (b) $N \simeq 5.9 \times 10^4$, $s \simeq 11.2$ and $T_c = 51.1\,$nK; $T = 33\,$nK for the gray line and $T = 37.4\,$nK for the dotted line. (c) $N \simeq 1.1 \times 10^5$, $s \simeq 16.7$, and $T_c = 63.0\,$nK; $T = 55\,$nK for the gray line and $T = 49.3\,$nK for the dotted line. (d) $N \simeq 2 \times 10^5$, $s \simeq 20$, and $T_c = 76.5\,$nK; $T = 73.4\,$nK for the gray line.

The "peak on a peak" features of interference patterns were confirmed by the measured linear densities of expanded atomic clouds in many runs of experiments. The black curves in Figs. 5(a)-5(c) display three typical density distributions which were obtained by integrating the pixels in each column of the corresponding absorption image. The calculated critical temperature T_c is usually in the order of several tens of nK. In contrast, during the evaporative cooling stage, the critical temperature for condensation in the QUIC trap is much higher ($\sim 400\,$nK). Actually, the experiment reported in [20] showed clearly a significantly decreased critical temperature for a combined trap when compared with a purely magnetic trap.

To test our theory, the temperature of the atomic sample before expansion must be known. It can be deduced from the transverse distribution of the normal gas after the TOF, which should take a Gaussian profile due to the initially thermal occupation of the transverse modes.
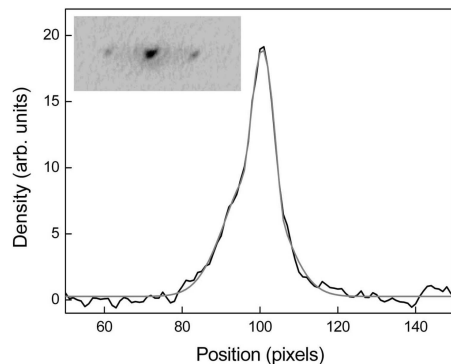

FIG. 6: Density distributions in the transverse dimension for the same atomic cloud as in Fig. 5(b). The black curve is the integration along the axial direction of the central peak. The gray curve is a bimodal fitting of the black curve, which represents a superposition of a Gaussian profile and a Thomas-Fermi profile (inverted parabola). The rms size of the Gaussian part gives a temperature of $37.4\,$nK. (Inset) The absorption image of this atomic cloud.

Since the condensate part should take a Thomas-Fermi profile in the transverse direction, a bimodal transverse distribution is expected for a released gas, just as shown in Fig. 6. However, a measured temperature based on this method usually has a large uncertainty due to the following reasons. First, in the transverse direction, the spatial extent of the condensate is not very distinct from that of the normal gas, especially when the condensate fraction is large. Second, the normal gas density profile deviates from an ideal Gaussian shape, and exhibits a slight asymmetry that may arise from the misalignment between the lattice light and the magnetic trap. Third, the optical noise in the absorption images also lowers the fitting accuracy. As pointed out in [21], an atomic sample can be significantly heated or cooled when adiabatically loaded to an optical lattice. Yet, to date, we have no alternative methods for accurate measurement of the temperature of an atomic sample confined in a lattice system. We have to treat temperature as a fitting parameter in the calculation, so that the calculated density distribution most closely reproduces the experimental curve.

The gray curves in Fig. 5 are the calculated density distributions of cold rubidium gases. Figure 5(a) is a case with a smaller atom number, and the fitting curve agrees fairly well with the experimental data. Figure 5(b) displays the interference pattern of another atomic sample initially confined in a deeper lattice, and the side peaks are more prominent. As a comparison, the atomic sample in Fig. 5(c) contains more atoms and the lattice depth was further increased. Accordingly, the calculated T_c shifts up to $63\,$nK. Since the normal gas density is increased, the feature of "peak on a peak" is more pronounced. In (b) and (c), we also plot the density distributions calculated using the measured temperature values. The larger deviation from the measured density profiles

should be attributed to the inaccuracy of temperature.

Despite the overall agreement between the theoretical and experimental curves in Fig. 5, there are still noticeable discrepancies. As the lattice depth increases, theoretical normal gas peaks become broader than the measured density profiles. As shown in Fig. 5(d), the gray line does not match the black curve, particularly at the wings of the normal gas. For this atomic sample, the temperature is close to T_c, and the condensate peaks are hence very small. The mismatch between the theory and experiment indicates that our model is not valid for very deep optical lattices. This can be easily understood by comparing the tunneling energy J to the energy offset between adjacent lattice sites induced by harmonic-potential. For a cloud with an extension of $l_M d$, this energy offset is $m\omega_z^2 d^2 l_M$ at the site of l_M. A typical value of $l_M = 200$ corresponds to an energy offset of $2\pi\hbar \times 16$ Hz, whereas J decreases with increased lattice depth. For $s = 20$ as in Fig. 5(d), $J \simeq 2\pi\hbar \times 10$ Hz. When J gets smaller than the energy offset between adjacent lattice sites, normal gas atoms are essentially localized and the semiclassical analysis breaks down. We have also calculated the T_c's for situations of $s \geq 20$, using the diagonalization method and semiclassical approximation, respectively. We do find significant discrepancy between the predictions of these two methods. In such situations, an atomic cloud should be treated as a chain of separate condensates, where the loss of condensate is interpreted as the loss of well-to-well phase coherence [17]. At a depth level of $s \simeq 30$, we observed a completely disappearance of interference peaks.

On the other hand, in our model, the interatomic interactions during TOF are taken into account for the subcondensates individually. This amounts to neglecting the variation of the wavefunction modulus induced by the interactions between subcondensates. The fluctuations of the wavefunction modulus are related to the relative phase of the subcondensates, and hence affect their phase coherence, leading to variations of the interference peak of the condensates. Evidently, the calculated condensate peaks are slightly wider than the measured ones (see Fig. 5). Perhaps, the neglected interactions are favorable for establishing a uniform phase which partially cancels the phase nonuniformity discussed in Sec. III B. Since we have not found a simple model to account for it, this effect will not be discussed in detail in this paper.

V. CONCLUSION

We have performed a study, both theoretically and experimentally, on the phase transition to macroscopic superfluidity for a Bose gas confined in a combined trap formed by a harmonic potential and an optical lattice. We have mainly investigated the interference patterns of the Bose gases below the critical temperature. By using a semiclassical energy spectrum and tight-binding approximation, we have derived an analytical approximation of the critical temperature which is applicable to an atomic gas residing in the vicinity of the bottom of the ground Bloch band. Furthermore, the interference patterns of the normal gas and the condensed gas were analyzed separately. We have derived the analytical expressions of the atomic density distribution for the released normal gas and condensed gas which has experienced a free expansion over a time of flight. Our calculation results show that a condensed gas is characterized by fully-resolved narrow interference peaks while a normal gas forms broad interference peaks with lower visibility. For comparison, we have performed a preliminary experiment using Bose-Einstein condensates of ^{87}Rb atoms. The combined trap system was implemented by applying a 1D optical lattice to a magnetically trapped condensate. The measured interference pattern agrees essentially with our theoretical prediction, exhibiting "peak on a peak" structures associated with the onset of condensed gases. Thus, both the theoretical and experimental results confirm that the "peak on a peak" structure is indeed a signature of macroscopic superfluidity in our inhomogeneous lattice system.

[1] M. Greiner, O. Mandel, T. Esslinger, T. W. Hansch, and I. Bloch, Nature **415**, 39 (2002).
[2] D. Jaksch, C. Bruder, J. I. Cirac, C. W. Gardiner, and P. Zoller, Phys. Rev. Lett. **81**, 3108 (1998).
[3] T. Stoferle, H. Moritz, C. Schori, M. Kohl, and T. Esslinger, Phys. Rev. Lett. **92**, 130403 (2004).
[4] R. B. Diener, Q. Zhou, H. Zhai, and T. L. Ho, Phys. Rev. Lett. **98**, 180404 (2007).
[5] Y. Kato, Q. Zhou, N. Kawashima, and N. Trivedi, Nature Physics **4**, 617 (2008).
[6] Min-Chul Cha, and Ji-Woo Lee, Phys. Rev. Lett. **98**, 266406 (2007).
[7] H. Kleinert, S. Schmidt, and A. Pelster, Phys. Rev. Lett. **93**, 160402 (2004).
[8] R. Ramakumar, and A. N. Das, Phys. Rev. B **72**, 094301 (2005).
[9] O. Zobay, and M. Rosenkranz, Phys. Rev. A **74**, 053623 (2006).

[10] B. G. Wild, P. B. Blakie, and D. A. W. Hutchinson, Phys. Rev. A **73**, 023604 (2006).

[11] R. Ramakumar, A. N. Das, and S. Sil, Eur. Phys. J. D **42**, 309 (2007).

[12] P. B. Blakie, and Wen-Xin Wang, Phys. Rev. A **76**, 053620 (2007).

[13] G.-D. Lin, Wei Zhang, and L.-M. Duan, Phys. Rev. A. **77**, 043626 (2008).

[14] I. B. Spielman, W. D. Phillips, and J. V. Porto, Phys. Rev. Lett. **100**, 120402 (2008).

[15] W. Zwerger, J. Opt. B: Quantum Semiclass. Opt. **5**, S9-S16 (2003).

[16] F. Dalfovo, S. Giorgini, L. P. Pitaevskii, and S. Stringari, Rev. Mod. Phys. **71**, 463 (1999).

[17] R. E. Sapiro, R. Zhang, and G. Raithel, New J. Phys. **11**, 013013 (2009).

[18] P. Pedri, L. Pitaevskii, S. Stringari, C. Fort, S. Burger, F. S. Cataliotti, P. Maddaloni, F. Minardi, and M. Inguscio, Phys. Rev. Lett. **87**, 220401 (2001).

[19] Th. Anker, M. Albiez, R. Gati, S. Hunsmann, B. Eiermann, A. Trombettoni, and M. K. Oberthaler, Phys. Rev. Lett. **94**, 020403 (2005).

[20] S. Burger, F.S. Cataliotti, C. Fort, P. Maddaloni, F. Minardi, and M. Inguscio, Europhys. Lett. **57**, 1 (2002).

[21] P. B. Blakie, and J. V. Porto, Phys. Rev. A **69**, 013603 (2004).